Original Article

Enhancement of LncRNA-HFRL expression induces cardiomyocyte inflammation, proliferation, and fibrosis via the sequestering of miR-149-5p-mediated collagen 22A inhibition

Xiaohua Li[1,2], Yun Teng[1,2], Miao Tian[1,2], Hailong Qiu[1,2], Junfei Zhao[1,2], Qiang Gao[1,2], Yong Zhang[1,2], Jian Zhuang[1,2], Jimei Chen[1,2]^

[1]Department of Cardiovascular Surgery, Guangdong Cardiovascular Institute, Guangdong Provincial People's Hospital, Guangdong Academy of Medical Sciences, Guangzhou, China; [2]Guangdong Provincial Key Laboratory of South China Structural Heart Disease, Guangdong Provincial People's Hospital, Guangdong Academy of Medical Sciences, Guangzhou, China

Contributions: (I) Conception and design: J Chen; (II) Administrative support: J Chen, J Zhuang; (III) Provision of study materials or patients: J Zhao, Q Gao, Y Zhang; (IV) Collection and assembly of data: X Li, Y Teng, M Tian, H Qiu; (V) Data analysis and interpretation: X Li, Y Teng, M Tian; (VI) Manuscript writing: All authors; (VII) Final approval of manuscript: All authors.

Correspondence to: Jimei Chen. Department of Cardiovascular Surgery, Guangdong Provincial People's Hospital, Guangdong Academy of Medical Sciences, Guangdong Cardiovascular Institute, 106 Zhong Shan Er Road, Guangzhou 510080, China. Email: jimei_1965@outlook.com.

Background: Long non-coding ribonucleic acids (lncRNAs) are believed to play crucial roles in cardiovascular diseases; however, details of the underlying mechanisms by which this occurs remain unclear.

Methods: A mouse heart failure (HF) model was established using isoproterenol (ISO), and confirmed by immunostaining and echocardiography. RNA-sequencing was performed to screen the differential lncRNA expression profiles and heart failure relative lncRNA (HFRL) was selected as the target which was validated by quantitative real-time polymerase chain reaction (qRT-PCR). In HL-1 cells, the cardiac function, inflammatory, and fibrosis-related genes expression changes were examined by qRT-PCR after silencing of HFRL by lentivirus. Meanwhile, Cell Counting Kit-8 (CCK-8) assays were used to detect the effects of HFRL on the cell proliferation and viability. Reactive oxygen species (ROS) assays were also used to explore the role of HFRL in oxidative damage. Next, bioinformatics analysis was conducted to predict the potential binding microRNAs (mmu-miR-149-5p) to HFRL, which was confirmed by RNA-pulldown assays. The target gene of miR-149-5p was also predicted and further validated by Dual-luciferase reporter assays, qRT-PCR, and western blot. To investigate the synergistic regulatory effect of HFRL and miR-149-5p, HL-1 cells were infected with the lentivirus of HFRL with or without simultaneous knockdown of miR-149-5p. Then, qRT-PCR and western blot were used to examine cardiac function, inflammatory, and fibrosis-related gene expression changes, respectively. In HL-1 cells, CCK-8 assays were performed to detect the proliferation and viability. ROS assays were used to explore the oxidative damage.

Results: The administration of ISO induced mice fibrosis, inflammation, and HF. The *in-vitro* results showed that knockdown of HFRL suppressed cardiomyocyte proliferation and viability, attenuated inflammatory, cardiac function, and fibrosis-related gene expression, and promoted oxidative damage. HFRL was found to bind to mmu-miR-149-5p and inversely target the 3'-untranscripted region of the collagen *22A1* gene. Thus, HFRL affected cardiomyocyte inflammation, proliferation, viability, oxidative damage, and pro-fibrotic function via sequestration to miR-149-5p.

Conclusions: The HFRL/miR-149-5p axis plays an important role in regulating cardiac inflammation, proliferation, and fibrosis via a synergistic effect, which suggests that HFRL might be a novel target for HF.

Keywords: Heart failure (HF); lncRNA-HFRL; miR-149-5p; Col 22A1

^ ORCID: 0000-0002-7866-7564.

Submitted Mar 04, 2022. Accepted for publication Apr 27, 2022.
doi: 10.21037/atm-22-1756
View this article at: https://dx.doi.org/10.21037/atm-22-1756

Introduction

Cardiovascular disease, which is accompanied by the onset of cardiac injury and fibrosis, is the main cause of mortality worldwide (1). Cardiac fibrosis is the most common adaptive response of the heart to external pressure or injury, including hypertension, myocardial infarction, and other disease-induced ventricular remodeling, which ultimately leads to heart failure (HF) (2,3). Despite great advances in the diagnosis and treatment of HF in decades, including the identification of a wide diversity of molecular targets, the effective therapeutic treatment of cardiac damage and fibrosis is limited and the mortality rate of HF continues to increase (4,5). Thus, a better understanding of the mechanistic molecular signaling of physiological and pathological cardiac injury and fibrosis will lead to the identification of novel therapeutic treatments and the eventual developments of novel anti-fibrotic and injury strategies for patients with HF.

Long non-coding ribonucleic acids (lncRNAs) have a length >200 nucleotides (nt) and no protein coding capacity (6,7). With the rapid development of high-throughput sequencing technology, more and more lncRNAs are being discovered and identified as important regulators of cardiovascular disease (8,9). Recently, emerging evidence has shown that lncRNAs are involved in regulating the occurrence and development of cardiac diseases via different signaling pathways, including cardiac hypertrophy, fibrosis, remodeling, and repair (10-12). LncDACH1 was found to be increased in diabetic cardiomyopathy mouse hearts and in high glucose-induced cardiomyocytes. The silencing of lncDACH1 expression has been shown to attenuate mitochondrial oxidative stress, cell apoptosis, cardiac fibrosis, and hypertrophy, and improve cardiac function in diabetic cardiomyopathy mice (13,14). The knockout of the lncRNA myocardial infarction associate transcript (MIAT) protects hearts from angiotensin II-induced hypertrophy and transverse aortic constriction-induced HF. Other studies speculated that the lncRNA MIAT controls advanced atherosclerotic lesion formation and plaque destabilization, as well as hypertrophy and heart failure (15,16). Additionally, the protective effect partially improves mouse heart calcium handling and contractility. LncRNA small nucleolar RNA host gene 1 (PVT1) promotes cardiomyocyte proliferation and improves cardiac function after myocardial infarction by forming a positive feedback loop with cellular myelocytomatosis (c-Myc) to sustain phosphatidylinositol-3-kinase and protein kinase B (PI3K/Akt) signaling activation, which contributes to cardiac regeneration (17).

Recently, lncRNAs have been reported to play crucial roles in cardiac disease development by competitively binding with micro RNAs (miRNAs) (18,19). A cardiomyocyte maturation-associated lncRNA controlled cardiomyocyte differentiation and maturation by binding with miR-1-1 and miR-133a2 via the NOTCH signaling pathway (20). LncRNA plasmacytoma variant translocation 1 interacts with miR-21-5p and alters mitochondrial fission and fusion in cardiomyocytes under hypoxia/reoxygenation injury *in vitro* and myocardial ischemia/reperfusion injury *in vivo* (21). As a competing endogenous RNA (ceRNA), lncRNA metastasis-associated lung adenocarcinoma transcript 1 was shown to sponge with miR-26b-5p and target mitofusin-1 (MFN1) to regulate mitochondrial dynamics and endothelial functions in the repair of cardiac microvascular dysfunction after myocardial infarction (18). However, the underlying mechanism of lncRNA in regulating cardiac damage and HF has not been clearly illustrated, and further research needs to be conducted to unveil the biological effect.

In the current study, using an isoproterenol (ISO)-induced mouse HF model and RNA-sequencing, we found a differentially expressed lncRNA in the mouse hearts, which we named HF-relative lncRNA (HFRL) and which was upregulated in the ISO-induced HF model *in vivo* and *in vitro*. In mouse cardiomyocytes (HL-1), the silencing of HFRL suppressed pro-inflammatory cytokine and pro-fibrotic genes and protein expression and cell proliferation. The bioinformatics analysis results suggested that HFRL binds to miR-149-5p targeted to COL22A1, which was confirmed by dual-luciferase assays. Additionally, our data showed that HFRL synergistically regulated mouse heart inflammation, damage and fibrosis by sequestering miR-149-5p targeted to COL22A1. Our study identified and verified a novel lncRNA-miRNA interaction network which can affect cardiomyocytes function. We present the

following article in accordance with the ARRIVE reporting checklist (available at https://atm.amegroups.com/article/view/10.21037/atm-22-1756/rc).

Methods

Agent

ISO was purchased from Sigma-Aldrich (USA). The kits for hematoxylin and eosin (H&E) and Masson trichrome staining were obtained from Abcam (Cambridge, UK). The following primary antibodies were used in our study: anti-phospho p65 (3033, CST), anti-cleaved caspase3 (9661, CST), anti-cleaved poly (ADP-ribose) polymerase (PARP) (9548, CST), anti-collagen I (ab21286, Abcam), anti-collagen III (ab7778, Abcam), anti-fibronectin (ab2413, Abcam), anti-collagen 22A1 (PA5-70816, Invitrogen, Carlsbad, USA), anti-alpha smooth muscle actin (anti-α-SMA) (A2547, Sigma, St. Louis, USA), and anti-glyceraldehyde-3-phosphate dehydrogenase (GAPDH) (39-8600, Invitrogen). Goat anti-mouse immunoglobin G (IgG) conjugated to Alexa Fluor 488 (ab150077, Abcam) or Alexa Fluor 594 (ab150116; Abcam) secondary antibodies were used for the immunofluorescence analysis.

Animals and HF models

A total of 24 male C57BL/6 mice (6 mice/cage, ~10 weeks old, ~30 g weight) obtained from Guangdong Medical Laboratory Animal Center were used in this study, and all the animal experiments were performed under a project license (No. KY-Z-2021-334-01) granted by the Ethics Committee of Guangdong Provincial People's Hospital, in compliance with the National Research Council (NRC) Guide for the Care and Use of Laboratory Animals (8th edition). The mice were housed in specific pathogen-free conditions at about 25 ℃ under a 12 h/12 h light-dark cycle with free access to food and water. Animal selection, model preparation, sample preparation, and the outcome analysis were conducted by different experimenters who were blinded to the grouping. A protocol was prepared before the study but was not registered.

The mice were randomly divided into the following 2 groups: (I) the phosphate buffer saline (PBS) control group (n=6); and (II) the ISO-HF group (n=18). In the PBS control group, the mice were administered phosphate buffer saline (PBS) by gavage for 3 weeks. In the ISO-HF group, the mice were randomly further divided into 3 subgroups (the 1-week subgroup, 2-week subgroup and 3-week subgroup), with 6 mice per subgroup. The mice were subcutaneously injected with ISO (5 mg/kg/day dissolved in PBS) for 1 week (the 1-week subgroup), 2 weeks (the 2-week subgroup), and 3 weeks (the 3-week subgroup). The mice in the 3 subgroups of the ISO-HF group were euthanized after receiving echocardiographic experiments on days 7, 14, and 21, respectively. Once resected from the mice, the hearts were washed with PBS and divided into 3 parts, 2 of which were stored at –80 ℃ for further messenger RNA (mRNA) and protein analysis. The left part was fixed with 4% (w/v) paraformaldehyde for the histological studies. No adverse events were observed during the experiment.

Histopathological analysis

The hearts of the HF and control mice were quickly dissected and fixed in 4% paraformaldehyde overnight, embedded in paraffin, sectioned into 5-μm thick slices and subjected to H&E and Masson's trichrome staining. All the analyses were conducted in accordance with the manufacturer's procedures (Abcam). The images were obtained with an Olympus BX53 microscope (Olympus, Japan). Masson's trichrome staining results were calculated as the percentage of the area occupied by fibrosis to the total area.

Echocardiography measurements

A Vevo2100 imaging ultrasound system (Visualsonics, Fujifilm, Canada) was used to evaluate the heart conditions of the mice. Two-dimensional and M-mode images were obtained in the short-axis view. The parameters, including the ejection fraction (EF%), fractional shortening (FS%) and left ventricular diastolic diameter (LVIDd), were measured and analyzed.

Immunohistochemistry

The paraffin sections were deparaffinized and rehydrated in accordance with standard protocols. After antigen retrieval using citrate buffer (ab93678, Abcam), the sections were blocked and probed with primary antibodies at 4 ℃ overnight. The following antibodies were used in this study: anti-collagen I (ab21286, 1:100) and anti-collagen III (ab7778, 1:100). Next, the sections were stained with a secondary antibody using a GTVisionTM III Detection System/Mo&Rb kit (GK500710, DAKO). Images were captured using an Olympus BX53 microscope (Olympus, Japan).

qRT-PCR

Total RNA was extracted from the heart tissues of the mice or HL-1 cells using TRIzol reagent (Invitrogen). Quantitative real-time polymerase chain reaction (qRT-PCR) was performed using the SYBR green master mix kit (TAKARA) on a Light Cycler 480 II system (Roche, Indianapolis, USA). The relative expression levels of the genes were determined and calculated based on the threshold cycle (Ct) value. The mRNA and lncRNA expression levels were normalized to GAPDH, and the miR-149-5p expression levels were normalized to U6. GAPDH or U6 was used as the internal control in each sample. The data were analyzed using the $2^{-\Delta\Delta CT}$ method.

RNA-sequencing

Total RNA was extracted from the mouse hearts and then treated with Deoxyribonuclease I (DNase I). The RNA-sequencing libraries were generated using the TruSeq kit and sequenced on a HiSeq 4000 system (Illumina, USA). The DESeq2 package was used to analyze the differentially expressed lncRNA genes. The genes with an adjusted P value <0.05 and log2 fold change >1 were defined as differentially regulated and then underwent an enrichment analysis with Cluster Profiler to detect which biological pathways were altered on CAV2 OE. The volcano plot shows the whole transcriptional changes across the groups, and a heatmap was plotted using the online tool ClustVis.

HL-1 cell culture and treatment

The mouse cardiomyocyte cell line HL-1 was purchased from the American Type Culture Collection (ATCC, USA) and cultured in Dulbecco's Modified Eagle Medium (Invitrogen) with 10% fetal bovine serum (GIBCO) and supplemented with 1% streptomycin at 37 ℃ in a 5% carbon dioxide atmosphere. To induce hypertrophy, the HL-1 cells were stimulated with ISO when cell confluence reached 50–60%. The cells were cultured with low serum (1%) medium for 16 h, and then 50 μM of ISO or PBS as the control was added for 24 h.

Lentivirus shRNA

The short-hairpin RNA (shRNA) for the knockdown of HFRL and a scrambled sequence as a control were synthesized by GenePharma (Shanghai, China) and inserted into the lentiviral vector pLKO. ShRNA lentiviruses were produced by co-transfecting 293 T cells with the lentivirus expression plasmid and packaging plasmid. The interference efficiency was determined by qRT-PCR.

Reactive oxygen species (ROS) assays

ROS assays were measured using a ROS assay kit (Beyotime, Beijing, China) in accordance with the manufacturer's protocol. In brief, the HL-1 cells were seeded on sterile glass cover slips into a 24-well plate. After treatment, the medium was removed and 10 μM of 2'-7'-dichlorofluorescein diacetate (DCFH-DA) solution with the fresh medium was added to each group well. The plate was incubated at 37 ℃ for 20 min, and after washing with PBS for 3 times, the immunofluorescence was analyzed and captured using a laser scanning confocal microscope (LSM 980, Zeiss, Jena, Germany).

Immunofluorescence

After treatment, the HL-1 cells on the sterile glass cover slips were fixed with 4% paraformaldehyde for 15 min at room temperature, and then permeabilized with 0.5% Triton. The cells were incubated with an anti-alpha smooth muscle actin (anti-α-SMA) antibody (1:50, A2547, Sigma) and anti-fibronectin (1:50, ab2413, Abcam) at 4 ℃ overnight. Next, the cells were incubated with a goat anti-mouse IgG conjugated to Alexa Fluor 488 (1:500, ab150077, Abcam) or Alexa Fluor 594 (1:500, ab150116; Abcam) secondary antibodies and kept at room temperature for 1 h. The cells were then washed, and the nuclei were counter stained with 4',6-diamidino-2-phenylindole (Roche Molecular Biochemicals) for 5 min at room temperature. Immunofluorescence was analyzed and captured using a laser scanning confocal microscope (LSM 980, Zeiss).

Cell proliferation and viability assay

Cell proliferation and viability were detected using a CCK-8 assay kit (Dojindo, Tokyo, Japan) in accordance with the manufacturer's protocol. In brief, the HL-1 cells were seeded into a 96-well plate (1×10^4 each well). After treatment, 10 μL of CCK-8 solution was added into each group well. The plate was incubated at 37 ℃ for 1 h, and the absorbance was measured at a 450-nm wavelength using a microplate reader (Molecular Device, USA).

Nuclear and cytoplasmic subcellular fractionation

The fractionation assays were performed using a Cytoplasmic and Nuclear RNA Purification Kit (NORGEN BIOTEK, Canada) in strict accordance with the manufacturer's procedures. Next, the qRT-PCR was used to detect the HFRL expression in nuclear and cytoplasmic extracts.

Small-interfering RNA and transfection

The MiR-149-5p mimics, inhibitor, and negative control (NC) were purchased from RiboBio. The HL-1 cells were seeded in a 6-well plate, and the transfection was carried out when the cell confluence reached 60%. MiRNA mimic or inhibitor (100 nM) was transfected into the HL-1 cells using Lipofectamine 3000 (Invitrogen) in accordance with the manufacturer's instruction. After 48 h, qRT-PCR and western blot assays were performed to examine the transfection efficiency.

Pull-down assay with biotinylated miRNA

The RNA-pulldown was performed using a kit (Thermo, Waltham, USA) in accordance with the manufacturer's instructions. Briefly, after the transection of biotinylated miRNA (100 nM), the HL-1 cells were harvested and incubated in lysis buffer on ice. The lysates were incubated with M-280 streptavidin magnetic beads (Sigma) and incubated at 4 ℃. After careful washing, the beads were harvested and the enrichment of HFRL were measured by qRT-PCR.

Western blotting

The proteins were extracted from the mouse heart tissues or HL-1 cells using ristocetin-induced platelet aggregation lysis buffer (Beyotime, Beijing, China). A total of 30 μg proteins were loaded and resolved by 10% sodium dodecyl sulfate polyacrylamide gel electrophoresis. After being transferred to polyvinylidene fluoride membranes (Millipore) and blocked with 5% non-fat milk, the membranes were probed with primary antibodies at 4 ℃ overnight. The following antibodies were used in this study: anti-collagen I (ab21286, 1:1,000), anti-collagen III (ab7778, 1:1,000), anti-fibronectin (ab2413, 1:1,000), anti-collagen 22A1 (PA5-70816, 1:1,000), anti-α-SMA (A2547, 1:1,000), and anti-GAPDH (39-8600, 1:2,000). Next, the membranes were incubated with horseradish peroxidase conjugated anti-mouse secondary antibodies (Promega, Madison, USA) for 1 h at room temperature. The signals were visualized with the ChemiDoc Touch Imaging System (BioRad, Hercules, USA) using an enhanced chemiluminescence kit (Pierce, Thermo). GAPDH served as the internal control.

Luciferase reporter assays

Collagen Type XXII Alpha 1 (COL22A1) 3'-untranscripted region (3'-UTR) containing the wild-type binding sites and mutation sequences of miR-149-5p were synthesized and inserted into the downstream of the luciferase gene in the pGL3 plasmid (Promega). Next, the luciferase vector (0.1 μg) was co-transfected with miR-149-5p mimics or NC into the HL-1 cells using Lipofectamine 3000 (Invitrogen). The renilla luciferase reporter (10 ng) was transfected as the control. Next, the cells were harvested after transfecting for 48 h, the dual-luciferase activities were measured by a luminometer in accordance with the manufacturer's instructions (Promega).

Statistical analysis

All the data are presented as the mean ± standard error of the mean. Significant differences between the groups were estimated by an independent-samples *t*-test or 1-way analysis of variance followed by a Bonferroni or Dunnett's *post-hoc* test for multiple group comparisons. A 2-tailed P value <0.05 was considered statistically significant. The data were analyzed using GraphPad Prism 8.0 and SPSS 18.0.

Results

LncRNA-HFRL is upregulated in the ISO-induced mouse hearts

Firstly, the HF mouse model was constructed by continually injecting ISO for 3 weeks. Next, the histological assay analysis was conducted to confirm the effect. Masson's staining revealed marked collagen deposition in the ISO-HF mice compared to the PBS control mice (see *Figure 1A*). Next, the cardiac function-related genes in the mouse hearts were detected by qRT-PCR. As *Figure 1B* shows, the expression levels of the hypertrophy markers genes (atrial natriuretic peptide: ANP; brain natriuretic peptide: BNP; and β-myosin heavy chain: β-MHC) were significantly increased under the effect of ISO. Additionally,

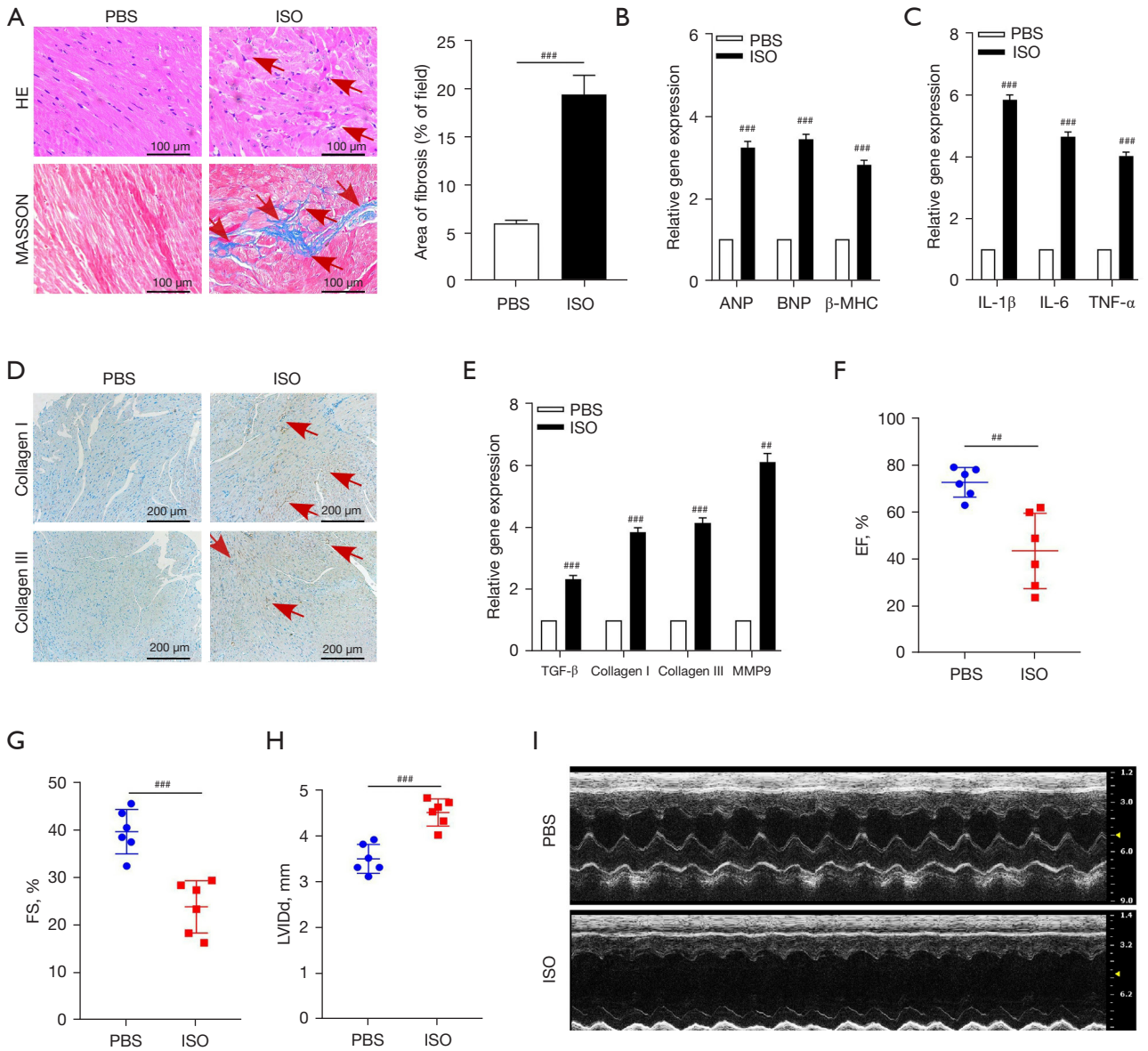

Figure 1 The administration of ISO induced mice cardiac inflammation, fibrosis, and disrupted function. (A) Representative images of H&E and Masson's trichrome staining showed the morphological changes in the mouse hearts. Scale bar is 100 μm. The fibrotic area of the ISO-induced mouse heart section was analyzed. The red arrows showed the morphological change in mice heart tissue. (B,C) qRT-PCR was used to detect the cardiac function genes and pro-inflammatory cytokine gene expression changes of the mouse hearts after being challenged by ISO; GAPDH was used as the internal control. (D) IHC staining showed the collagen I and collagen III protein expression changes of mouse hearts. The red arrows depicted the positive staining in mice heart tissue sections. Scale bar is 200 μm. (E) qRT-PCR was applied to examine the TGF-β, collagen I, collagen III, and MMP9 gene expression changes of the mouse hearts; GAPDH was used as the internal control. (F-I) Mice cardiac function was evaluated by measuring the EF, FS, and LVIDd by echocardiography. $^{\#\#}$, P<0.01; $^{\#\#\#}$, P<0.001. PBS, phosphate buffer saline; ISO, isoproterenol; H&E, hematoxylin and eosin; ANP, atrial natriuretic peptide; BNP, brain natriuretic peptide; β-MHC, β-myosin heavy chain; IL, interleukin; TNF-α, tumor necrosis factor alpha; EF, ejection fraction; FS, fractional shortening; LVIDd, left ventricular diastolic diameter; qRT-PCR, quantitative real-time polymerase chain reaction; GAPDH, glyceraldehyde-3-phosphate dehydrogenase; IHC, immunohistochemistry.

pro-inflammatory cytokine gene expression was also increased under the effect of ISO (see *Figure 1C*). The protein expression levels of collagen I and collagen III and the f ibrosis-related gene, including of: transforming growth factor β (TGF-β), collagen I, collagen III and matrix metalloproteinase 9 (MMP9), were detected using IHC and qRT-PCR, respectively. The results indicated that fibrosis-related gene and protein expression level were remarkably increased in the ISO-HF mouse hearts (see *Figure 1D,1E*).

We then assessed the cardiac function of the mouse hearts by measuring the EF, FS, and LVIDd by echocardiography. As *Figure 1F-1I* show, compared to the PBS administration control group mice, the cardiac function of the mouse hearts in the ISO-induced HF mice group was severely impaired, as indicated by the reduced dimensions of EF and FS, and the increased dimensions of the LVIDd.

To identify the differentially expressed lncRNAs involved in the regulation of the heart fibrosis and the HF process, RNA-sequencing was conducted. The results showed that 119 genes were upregulated, and 93 genes were downregulated in the ISO-treated mouse hearts. A volcano map shows all the differentially expressed lncRNAs and a heat map shows the top 50 genes (see *Figure 2A,2B*). Among these differentially expressed genes (DEGs) (Padj<0.05), 10 lncRNAs were significantly dysregulated in the mouse hearts after ISO treatment, and qRT-PCR was performed to verify the expression profiles. Among the 10 lncRNAs, the expression of NONMMUG088802 was significantly enhanced in the ISO-treated mice (see *Figure 2C*). Additionally, its expression level was significantly increased in mouse hearts induced by ISO (see *Figure 2D*). Thus, we focused on NONMMUG088802 as the research target in our subsequent experiments and renamed this lncRNA the HFRL.

Knockdown of HFRL suppresses cardiac function, inflammatory, fibrosis-related gene expression, and proliferation in the HL-1 cells

To further examine the function of HFRL in regulating cardiac fibrosis, we knocked down HFRL in the mouse cardiomyocyte HL-1 cells using a lentivirus carrying a HFRL-specific short-hairpin RNA (LV-sh-HFRL). The silencing efficiency was first detected using qRT-PCR. Next, ISO was added to the HL-1 cells to further evaluate the function of HFRL. As *Figure 3A* shows, ISO significantly enhanced the HFRL expression levels in HL-1 cells, while the shRNA efficiently inhibited the HFRL expression levels compared to those of the NC group (LV-sh-NC). Next, the function of HFRL was measured, and we found that exposure to ISO increased the expression of the hypertrophy markers (ANP, BNP, and β-MHC) and pro-inflammatory cytokine gene expression (TNF-α, IL-1β, and IL-6) in the HL-1 cells. However, the silencing of HFRL expression suppressed the ANP, BNP, β-MHC, TNF-α, IL-1β, and IL-6 gene expression under the effect of ISO (see *Figure 3B,3C*).

We also explored the effects of HFRL on cardiomyocyte proliferation and viability, and as *Figure 3D,3E* show, the viability and proliferative ability were diminished under the effect of ISO, while the knockdown of HFRL expression partially rescued HL-1 cell viability and proliferation. Additionally, ISO triggered HL-1 cell oxidative damage, as the ROS level increased after being challenged by ISO. However, the knockdown of HFRL decreased the ROS production level (see *Figure 3F*). We also examined the fibrosis-related gene and protein expression changes after the silencing of HFRL in HL-1 cells. As *Figure 3G* shows, the inhibition of HFRL expression impaired α-SMA and fibronectin (FN) expression. Additionally, ISO upregulated TGF-β, collagen I, collagen III, α-SMA, FN, and *MMP9* gene expression. However, silencing HFRL expression partially attenuated fibrosis-related gene expression under the effect of ISO in HL-1 cells (see *Figure 3H*).

HFRL directly binds with miR-149-5p in HL-1 cells

There is increasing evidence that lncRNAs participate in the initiation and progression of cardiovascular diseases, such as cardiac hypertrophy and fibrosis. Many cytoplasmic lncRNAs have been reported to act as ceRNAs by competitively binding to specific miRNAs. We first examined the subcellular localization of HFRL in the HL-1 cells, and observed that HFRL was predominantly distributed in the cytoplasm (see *Figure 4A*). To explore whether miRNAs bind to HFRL and mediate the function of HFRL in cardiac fibrosis in our study, a bioinformatics analysis was performed to predict the miRNAs that may contain complementary pairing sequences with HFRL using the online software RegRNA 2.0 database (http://regrna.mbc.nctu.edu.tw/html/prediction.html). In accordance with the prediction results, a series of miRNAs was found to have potential binding sites to HFRL. To determine which miRNA was the most promising, lentivirus was

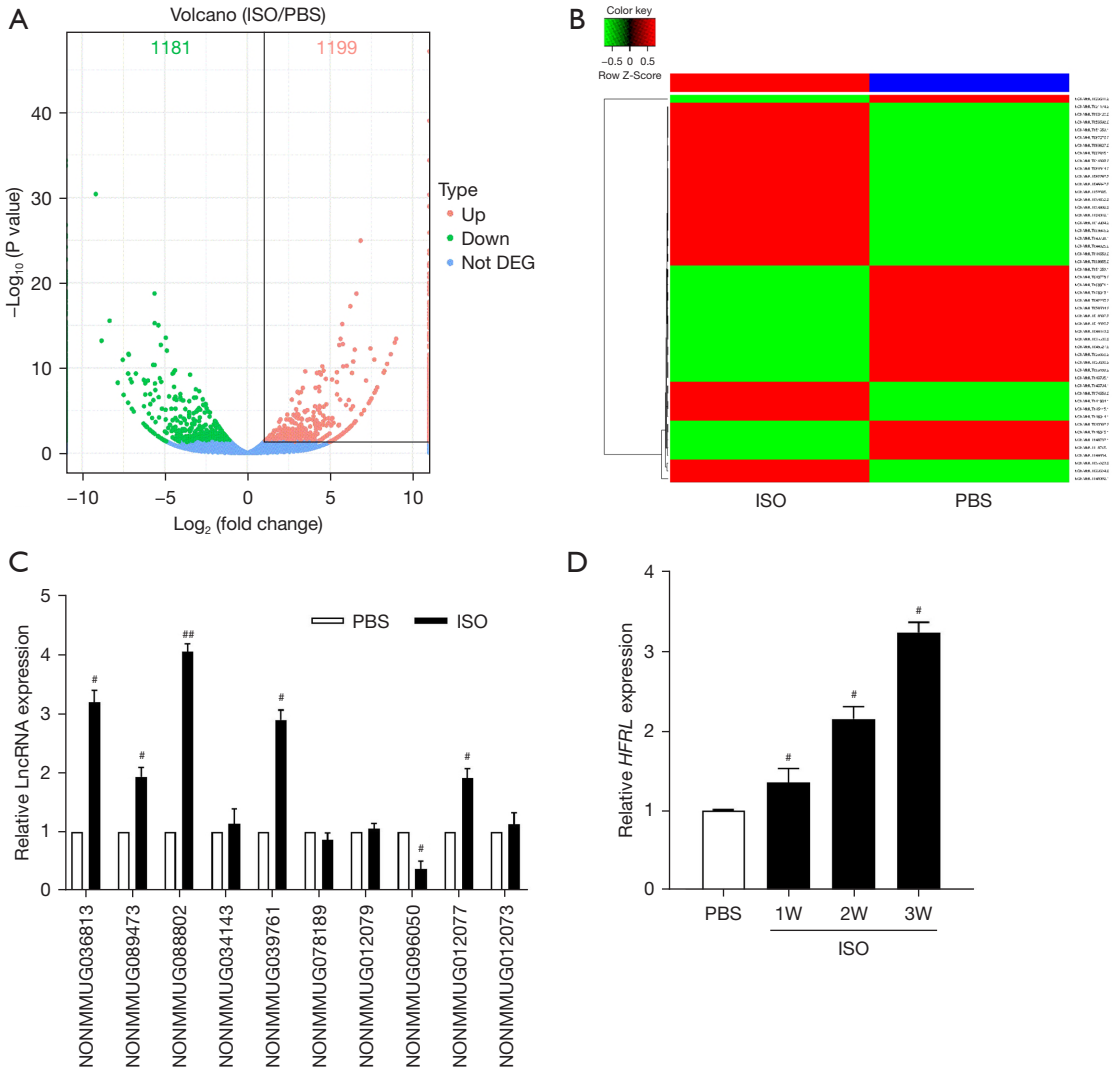

Figure 2 LncRNA-HFRL was upregulated in the ISO-induced mouse hearts. RNA-sequencing was performed to screen the differentially expressed lncRNAs. (A) Volcano plot showing the whole differentially expressed lncRNA genes. (B) Heatmap showing the top 50 most differentially expressed lncRNAs. (C) The top 10 most differentially expressed lncRNAs detected by qRT-PCR. (D) The expression of HFRL was increased treated by ISO. #, P<0.05; ##, P<0.01. PBS, phosphate buffer saline; W, week; ISO, isoproterenol; DEG, differentially expressed gene; LncRNA, long non-coding ribonucleic acids; HFRL, heart failure-relative lncRNA; qRT-PCR, quantitative real-time polymerase chain reaction.

used to silence HFRL expression in HL-1 cells and qRT-PCR was applied to examine the expression changes of miRNAs. As *Figure 4B* shows, miR-149-5p was the most upregulated one of all miRNAs, and HFRL contained a complementary sequence for miR-149-5p (see *Figure 4C*). We further examined the expression of miR-149-5p in the ISO-induced HF mouse hearts and found that miR-149-5p was significantly decreased after ISO administration as compared to the PBS application (see *Figure 4D*). Additionally, miR-149-5p was continuously downregulated from day 7 to day 21 after ISO injection (see *Figure 4E*). To confirm whether HFRL could directly bind to miR-149-5p, we applied a biotin-avidin pull-down assay to test whether miR-149-5p could pull down HFRL. The HL-1 cells were transfected with biotinylated wild-type miR-149-5p (Bio-149-5p-wt) or mutant miR-149-5p (Bio-149-5p-mut). The cells were then harvested and measured by qRT-PCR. Our results showed that HFRL was pulled down and enriched

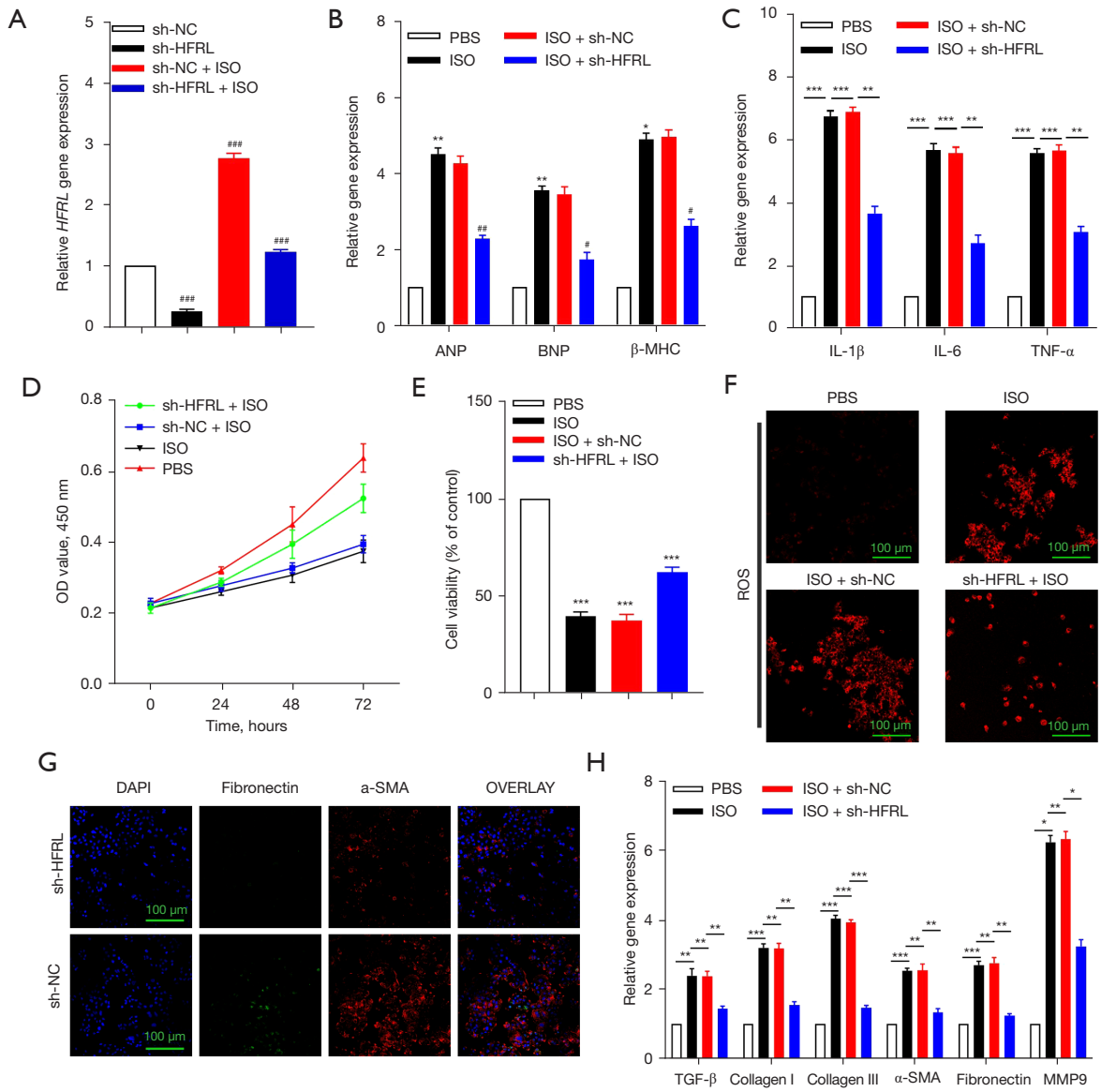

Figure 3 The knockdown of HFRL suppressed cardiac inflammation, proliferation, oxidative damage, and fibrosis induced by ISO in HL-1 cells. (A) The silencing efficiency of shRNA to HFRL was examined by qRT-PCR in the HL-1 cells; GAPDH was used as the internal control. (B,C) qRT-PCR was used to detect the cardiac function genes and pro-inflammatory cytokine gene expression changes after the silencing of HFRL using shRNA and triggered by ISO in the HL-1 cells; GAPDH was used as the internal control. (D,E) CCK-8 assays were performed to measure the HL-1 cell viability and proliferative ability changes after the knockdown of HFRL expression using shRNA and inducing by ISO. (F) ROS assays were carried out to examine oxidative damage after inhibiting HFRL expression and being challenged by ISO in the HL-1 cells. The representative images were visualized and captured using a laser scanning confocal microscope and the scale bar is 100 μm. (G) Immunofluorescence staining showed that the silencing of HFRL inhibited α-SMA and fibronectin expression. Scale bar is 100 μm. (H) qRT-PCR was applied to detect the expression of fibrosis-related genes (TGF-β, collagen I, collagen III, α-SMA, fibronectin, and MMP9) induced by ISO in the HL-1 cells after the silencing of HFRL expression; GAPDH was used as the internal control. $^{\#}$, P<0.05; $^{\#\#}$, P<0.01; $^{\#\#\#}$, P<0.001; *, P<0.05; **, P<0.01; ***, P<0.001. NC, negative control; HFRL, heart failure-relative lncRNA; ISO, isoproterenol; PBS, phosphate buffer saline; ANP, atrial natriuretic peptide; BNP, brain natriuretic peptide; β-MHC, β-myosin heavy chain; IL, Interleukin; TNF-α, tumor necrosis factor alpha; OD, optical density; ROS, reactive oxygen species; DAPI, 4',6'-diamidino-2-phenylindole; α-SMA, alpha smooth muscle actin; GAPDH, glyceraldehyde-3-phosphate dehydrogenase; qRT-PCR, quantitative real-time polymerase chain reaction; CCK-8, Cell Counting Kit-8.

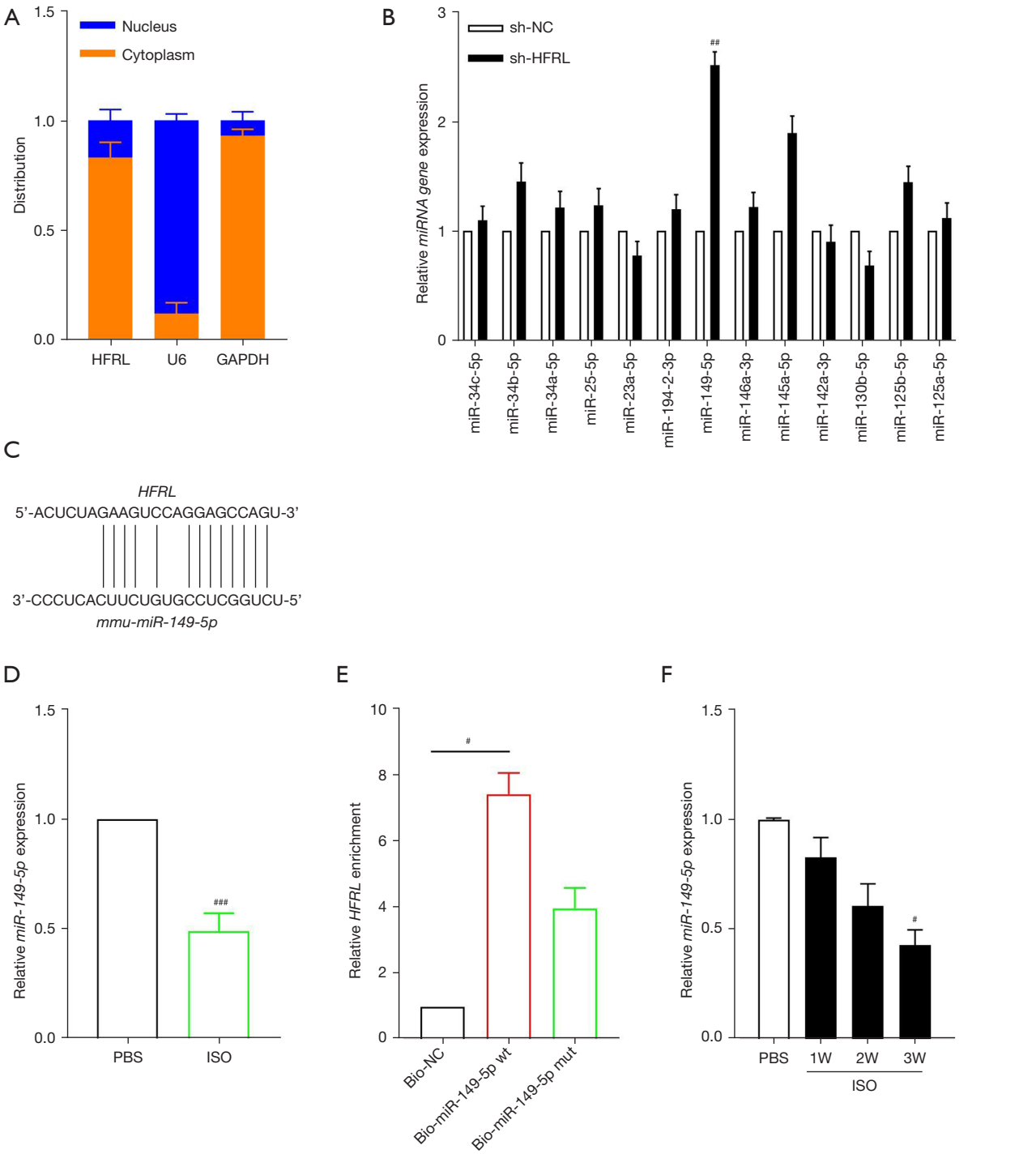

Figure 4 HFRL directly binds with miR-149-5p in cardiomyocytes. (A) Subcellular fractionation assays showed that HFRL was mainly located in the cytoplasm of the HL-1 cells. (B) Knockdown of HFRL expression and qRT-PCR was performed to detect the miRNA expression changes. U6 was used as the internal control. (C) The predictive binding sequences. (D) MiR-149-5p was downregulated in ISO-treated mouse hearts as detected by qRT-PCR. U6 was used as the internal control. (E) RNA-pulldown assays were conducted to directly explore the binding between HFRL and miR-149-5p. (F) MiR-149-5p was downregulated in ISO-induced HF mouse hearts. U6 was used as the internal control. $^{\#}$, P<0.05; $^{\#\#}$, P<0.01; $^{\#\#\#}$, P<0.001. HFRL, heart failure-relative lncRNA; GAPDH, glyceraldehyde-3-phosphate dehydrogenase; NC, negative control; W, week; ISO, isoproterenol; PBS, phosphate buffer saline; qRT-PCR, quantitative real-time polymerase chain reaction; HF, heart failure.

by the wild-type miR-149-5p but not by the mutant miR-149-5p (see *Figure 4F*), which suggests that HFRL directly binds with miR-149-5p in HL-1 cells.

COL22A1 is the target of miR-149-5p in HL-1 cardiomyocytes

It is well known that miRNA regulates gene expression by binding with the 3'-UTR of target gene. Next, 2 online bioinformatics software databases, TargetScan (http://www.targetscan.org/vert_72/) and PicTar (https://pictar.mdc-berlin.de/), were used to predict the candidate targets containing the potential complementary binding sites to miR-149-5p. In accordance with the search results, we found a binding sequence in the 3'-UTR COL22A1 for miR-149-5p (see *Figure 5A*). To confirm the target relationship between miR-149-5p and COL22A1, the mimics and inhibitor of miR-149-5p were used in the HL-1 cells. As *Figure 5B*,*5C* show, the forced expression of miR-149-5p significantly suppressed COL22A1 gene and protein expression, while the knockdown of miR-149-5p resulted in the upregulation of COL22A1 both in the genes and proteins as compared to the miRNA mimics and inhibitor NC. We further constructed a luciferase reporter vector containing the miR-149-5p wild-type or mutant binding sequences of COL22A1. The luciferase assays showed that miR-149-5p inhibited the activities of the wild-type COL22A1 luciferase vector but had no effect on the mutated COL22A1 luciferase vector (see *Figure 5D*). Next, the gene and protein of the COL22A1 expression level was detected in an ISO-induced mouse heart, and the results showed that both the gene and protein were significantly more enhanced in the ISO-treated mice than the PBS-treated mice (see *Figure 5E*,*5F*).

HFRL and miR-149-5p synergistically regulates cardiac function, inflammation, proliferation, and fibrosis

We then examined whether miR-149-5p mediated the regulatory effect of HFRL on cardiac function in HL-1 cells. As *Figure 6A-6G* show, the administration of ISO increased HL-1 cardiac function and pro-inflammatory-related gene expression, impaired HL-1 cell proliferation and viability, increased ROS production, and promoted pro-fibrotic genes and protein expression (COL22A1, collagen I, collagen III, α-SMA, and Fn), and apoptosis marker expression (cleaved caspase3, and PARP). Conversely, the knockdown of HFRL by shRNA attenuated HL-1 cardiac function and pro-inflammatory-related gene expression, enhanced HL-1 cell proliferation and viability, decreased ROS production, and prohibited pro-fibrotic genes and protein expression (COL22A1, collagen I, collagen III, α-SMA, and FN), and apoptosis marker expression (cleaved caspase3 and PARP). However, the inhibition effect of HFRL on HL-1 was partially rescued by the simultaneous silencing of miR-149-5p, indicating that HFRL and miR-149-5p synergistically regulated cardiac function, inflammation, proliferation, and fibrosis in the HL-1 cells.

Discussion

Cardiovascular diseases always cause HF and may even lead to mortality (22). The high and increasing mortality and morbidity rates of cardiovascular disease have created a socio-economic burden (23). Despite great advances in therapeutic approaches and drug treatments in the last decades, effective curative treatments of HF remain limited (24,25). Thus, it is urgent and essential to identify novel targets and develop new curative treatments for HF.

LncRNAs have been shown to be involved in a series of diseases, such as tumorigenesis and cardiovascular disease (26,27). However, little is known about the role and mechanism of lncRNAs in the process of cardiac inflammation and fibrosis. Recently, a lncRNA cardiac physiological hypertrophy-associated regulator was shown to induce cardiac physiological hypertrophy and promote functional recovery after myocardial ischemia-reperfusion injury (28). LncRNA scaffold attachment factor B interacting lncRNA (SAIL) regulates cardiac fibrosis by regulating the scafold attachment factor B (SAFB)-mediated transcription of fibrotic-related genes (29). LncRNA safely contributes to cardiac fibrosis through the Safe-Sfrp2-HuR complex in myocardial infarction *in vivo* and *in vitro* (30).

In this study, we first constructed heart failure mice model induced by ISO and verified by histopathology, ultrasound imaging and molecular biological methods. Through RNA-sequencing and qRT-PCR, we found and identified a novel lncRNA-HFRL that was significantly upregulated in the HF mouse hearts as induced by ISO. Our results indicated that the knockdown of HFRL expression suppressed inflammation, proliferation, viability, and fibrogenesis *in vitro*. Additionally, we also examined the underlying molecular mechanism of HFRL-regulated cardiac fibrosis, and found that the expression level of HFRL was significantly accelerated in the ISO-induced mouse hearts and HL-1 cells. More importantly, the pro-

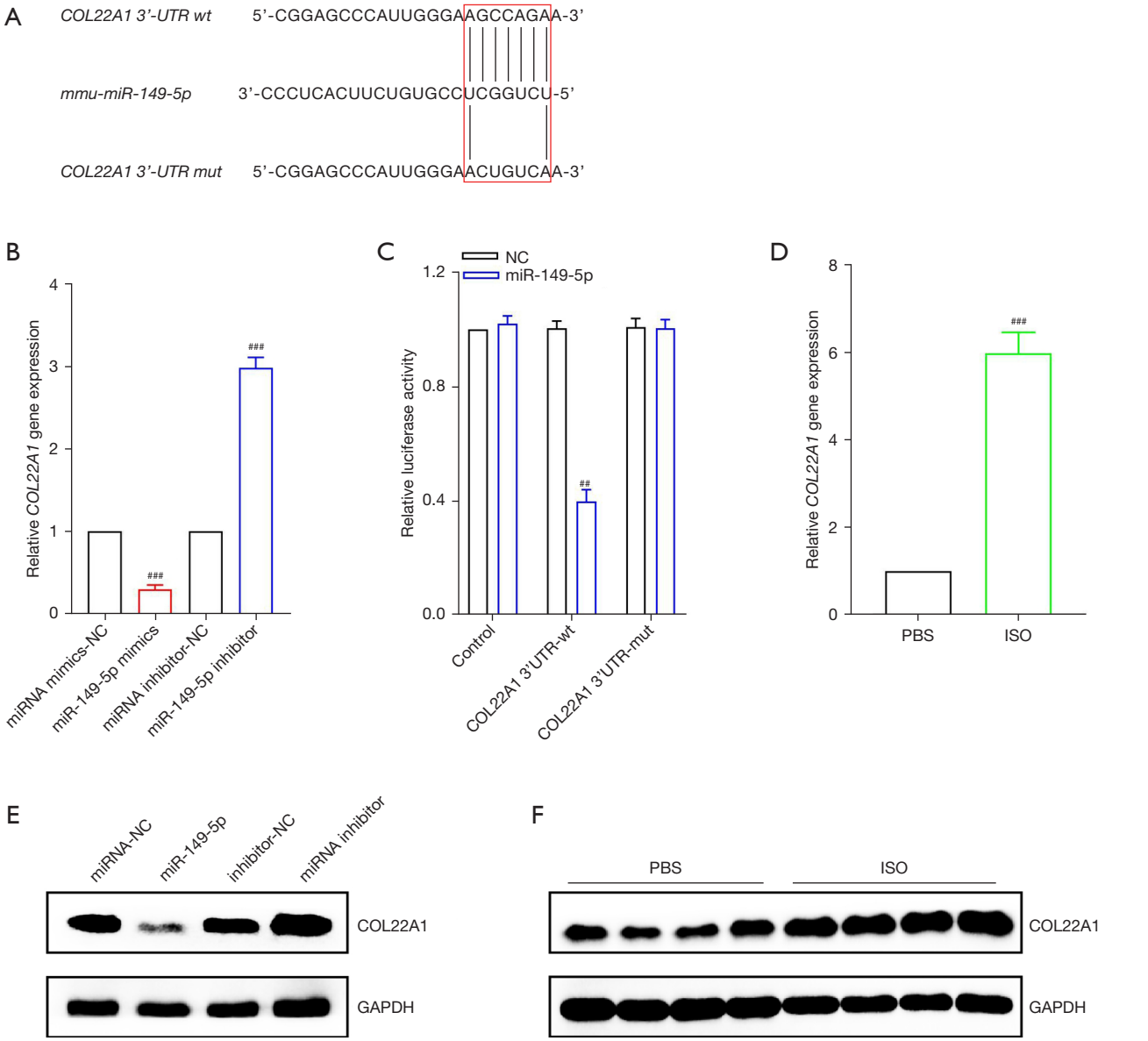

Figure 5 COL22A1 is the target of miR-149-5p in HL-1 cells. (A) The predictive binding sequences between miR-149-5p and COL22A1. (B,C) The qRT-PCR and western blot assays showed that the overexpression of miR-149-5p significantly suppressed *COL22A1* gene and protein expression, while the inhibition of miR-149-5p resulted in the upregulation of COL22A1 both in gene and protein as compared to the miRNA mimics and inhibitor NCs; U6 and GAPDH were used as the respective internal controls for each. (D) Luciferase assays were applied to confirm the binding between miR-149-5p and the 3'-UTR of COL22A1. Luciferase activity was measured. (E,F) qRT-PCR and western blot assays were performed to examine the mRNA and protein expression of COL22A1 in the mouse hearts induced by ISO or control; GAPDH was used as the internal control. ##, P<0.01; ###, P<0.001. NC, negative control; PBS, phosphate buffer saline; ISO, isoproterenol; GAPDH, glyceraldehyde-3-phosphate dehydrogenase; qRT-PCR, quantitative real-time polymerase chain reaction.

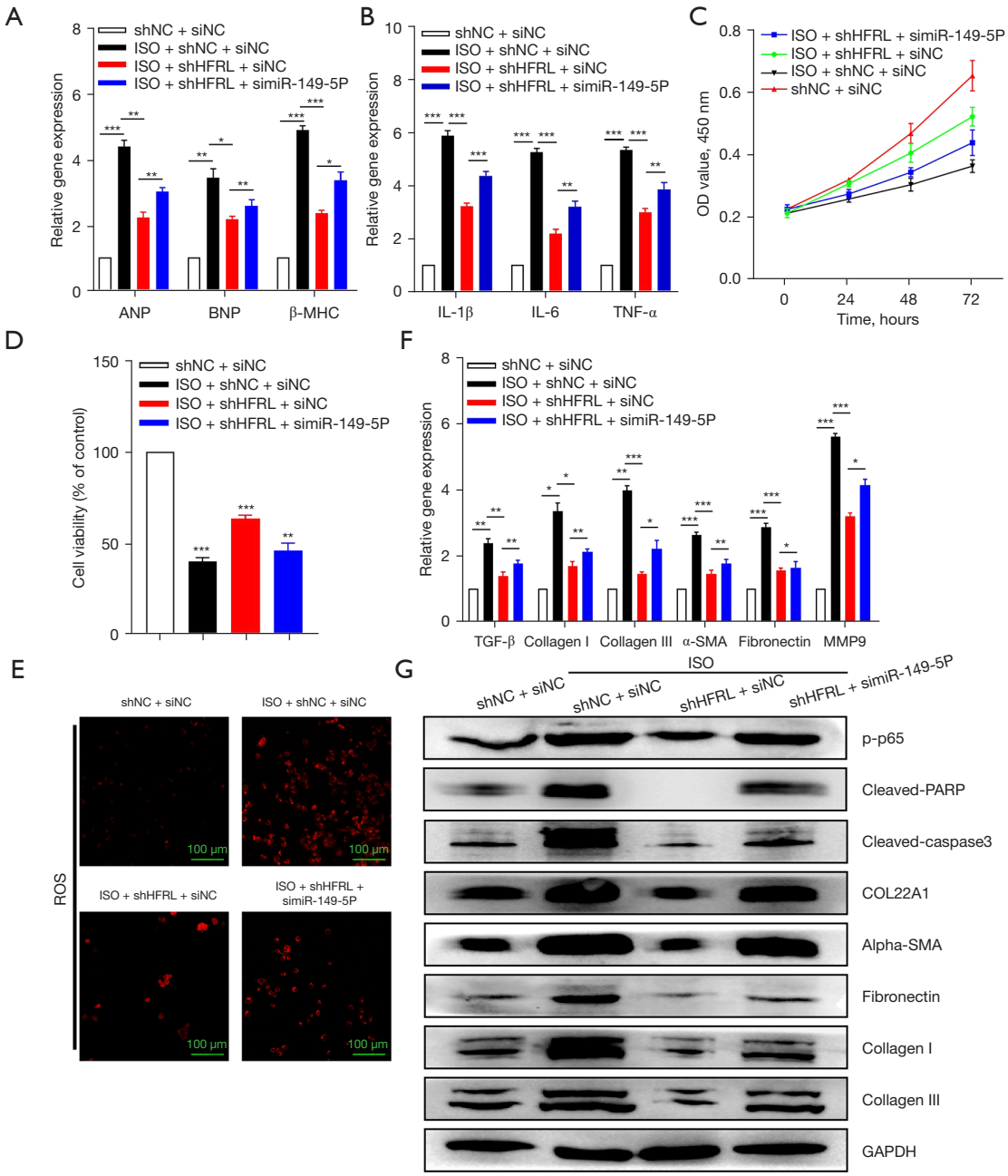

Figure 6 HFRL and miR-149-5p synergistically regulated cardiac inflammation, oxidative damage, proliferation, and fibrosis. (A-G) The qRT-PCR, CCK-8, ROS, and western blot assays showed that the knockdown of HFRL by shRNA attenuated HL-1 cardiac function and pro-inflammatory related gene expression, enhanced HL-1 cell proliferation and viability, decreased ROS production, and prohibited pro-fibrotic genes and protein expression (i.e., COL22A1, collagen I, collagen III, α-SMA, and FN), and apoptosis marker expression (i.e., cleaved caspase3, and PARP). The inhibition effect of HFRL on HL-1 was partially rescued by the simultaneous silencing of miR-149-5p, indicating that HFRL and miR-149-5p synergistically regulated cardiac function, inflammation, proliferation, and fibrosis in HL-1 cells. ROS assays were performed to detect HL-1 cells oxidative damage after treatment. Then, the immunofluorescence was analyzed and captured using a laser scanning confocal microscope and the scale bar is 100 μm. *, P<0.05; **, P<0.01; ***, P<0.001. NC, negative control; HFRL, heart failure-relative lncRNA; ISO, isoproterenol; ANP, atrial natriuretic peptide; BNP, brain natriuretic peptide; β-MHC, β-myosin heavy chain; IL, Interleukin; TNF-α, tumor necrosis factor alpha; ROS, reactive oxygen species; GAPDH, glyceraldehyde-3-phosphate dehydrogenase; qRT-PCR, quantitative real-time polymerase chain reaction; CCK-8, Cell Counting Kit-8; FN, fibronectin; PARP, poly (ADP-ribose) polymerase.

fibrotic effect of HFRL was mediated by the sequestration and downregulation of miR-149-5p. Further, miR-149-5p was downregulated in the ISO-induced mouse hearts.

Previous research has shown that the dysregulation of miR-149-5p is closely associated with malignant tumor progression, metastasis, and chemoresistance in gastric cancer (31-33), papillary thyroid cancer (34), colorectal cancer (35-37), and breast cancer (38). Additionally, miR-149-5p is also involved in the pathogenesis of inflammation-associated diseases, such as the $PM_{2.5}$-induced inflammatory response (39), rheumatoid arthritis (40), and chronic obstructive pulmonary disease (41). In recent years, it has been reported that miR-149-5p plays crucial roles in cardiovascular diseases. Macrophage-derived miR-149-5p targeting CD47 was shown to regulate the development of necrotic atherosclerotic plaques (42). Further, miR-149-5p was shown to regulate the development of hepatic fibrosis by targeting TGF-β2 *in vivo* and *in vitro* (43). However, little is known about the role and function of miR-149-5p in cardiac function, inflammation, and fibrosis. In the current study, miR-149-5p was identified as an anti-inflammation and fibrotic miRNA, and the decreased expression relieved the repression of COL22A1. Additionally, the inhibition of miR-149-5p partially released the sponge action of HFRL and enhanced COL22A1 expression. Our study elucidated the anti-inflammation and fibrotic effect of miR-149-5p in cardiac function, inflammation, and fibrosis, and suggests that the targeting of miR-149-5p may be a novel therapeutic strategy for the treatment of cardiac function, inflammation, and fibrosis.

CeRNA is considered an important mechanism by which lncRNAs regulate biological activities by competitive binding with specific miRNAs (6). There is emerging evidence that lncRNAs play pivotal roles in cardiovascular disease, including organ injury and fibrosis, development by functioning as ceRNAs to bind with miRNAs (44,45). For example, serum extracellular vesicles carrying lncRNA MIAT induce atrial injury, inflammation, and fibrosis to promote atrial remodeling and atrial fibrillation via sponging to miR-485-5p (46). The upregulation of lncRNA DCRF increases myocardial fibrosis, injury, and the acceleration of cardiomyocyte autophagy levels by acting as a ceRNA to sponge with miR-551b-5p (47).

COL22A1 has rarely been examined in previous studies. It was first identified as a novel specific component of tissue junctions that can act as a cell adhesion ligand for skin epithelial cells and fibroblasts (48). The silencing of the *col22a1* gene in zebrafish resulted in muscular dystrophy, destroying the myotendinous junction (49). Another study reported that as a TGFβ early response gene, COL22A1 mediated the fibroblast to myofibroblast transition in human skin systemic sclerosis dermal fibrosis model (50). However, only a few studies have been conducted on the role of COL22A1 in cardiovascular disease, especially in the process of cardiac function, fibrosis, and injury. Our study revealed that COL22A1 was upregulated in the HF mouse hearts and mediated the cardiac function, inflammation, and fibrosis process.

Although it has been well recognized that lncRNAs played pivotal roles in cardiac disease development. The biggest problem and challenge that need to be overcome in the clinical application of lncRNA is that most of lncRNAs have no homologues between human and mice, which limited the importance and significance of lncRNA research, including of the therapeutic drugs and treatment strategy development. In the current study, we failed to find the homolog of the lncRNA-HFRL in the human genome, which limits the clinical value of our study to some extent. However, there are few reports on the role of miR-149-5p and COL22A1 in cardiomyocyte function and our results suggest the protection of miR-149-5p on heart failure. More research on the function and effect of HFRL/miR-149-5p and COL22A1 signaling pathway needs to be conducted in the future.

In conclusion, in this study, we observed and demonstrated that both lncRNA-HFRL and COL22A1 shared the same binding sites with miR-149-5p; thus, we speculated that HFRL binds and interacts with miR-149-5p, which in turn inversely blocks its negative regulation to its target of COL22A1. Thus, in accordance with our results, we surmised that in the HF mice model, the acceleration of HFRL competitively binds with miR-149-5p, and then alleviates the inhibitory effects of miR-149-5p on COL22A1, which promotes inflammation, injury, and fibrogenesis. These findings indicate that interfering with HFRL may provide a novel strategy for protecting heart function from cardiac fibrosis and injury in the future.

Acknowledgments

The authors would like to thank all the fellows in the Department of Cardiovascular Surgery, Guangdong Cardiovascular Institute, Guangdong Provincial People's Hospital.

Funding: This work was supported by the Guangdong Medical Science and Technology Research Foundation (No.

A2020029, to Xiaohua Li), the National Key Research and Development Program of China (No. 2018YFC1002600, to Jimei Chen); the Guangdong Peak Project (No. DFJH2019, to Jimei Chen), the Science and Technology Planning Project of Guangdong Province, China (Nos. 2019B020230003, 2017B090904034, 2017B030314109, and 2018B090944002, to Jian Zhuang); the Guangdong Peak Project (No. DFJH201802, to Jian Zhuang), and the National Natural Science Foundation of China (No. 82000081, to Junfei Zhao).

Footnote

Reporting Checklist: The authors have completed the ARRIVE reporting checklist. Available at https://atm.amegroups.com/article/view/10.21037/atm-22-1756/rc

Data Sharing Statement: Available at https://atm.amegroups.com/article/view/10.21037/atm-22-1756/dss

Conflicts of Interest: All authors have completed the ICMJE uniform disclosure form (available at https://atm.amegroups.com/article/view/10.21037/atm-22-1756/coif). The authors have no conflicts of interest to declare.

Ethics Statement: The authors are accountable for all aspects of the work in ensuring that questions related to the accuracy or integrity of any part of the work are appropriately investigated and resolved. The animal experiments were performed under a project license (No. KY-Z-2021-334-01) granted by the Ethics Committee of Guangdong Provincial People's Hospital, in compliance with the National Research Council (NRC) Guide for the Care and Use of Laboratory Animals (8th edition).

References

1. Roth GA, Mensah GA, Johnson CO, et al. Global Burden of Cardiovascular Diseases and Risk Factors, 1990-2019: Update From the GBD 2019 Study. J Am Coll Cardiol 2020;76:2982-3021.
2. Zhou B, Perel P, Mensah GA, et al. Global epidemiology, health burden and effective interventions for elevated blood pressure and hypertension. Nat Rev Cardiol 2021;18:785-802.
3. Vogel B, Acevedo M, Appelman Y, et al. The Lancet women and cardiovascular disease Commission: reducing the global burden by 2030. Lancet 2021;397:2385-438.
4. López B, Ravassa S, Moreno MU, et al. Diffuse myocardial fibrosis: mechanisms, diagnosis and therapeutic approaches. Nat Rev Cardiol 2021;18:479-98.
5. González A, Schelbert EB, Díez J, et al. Myocardial Interstitial Fibrosis in Heart Failure: Biological and Translational Perspectives. J Am Coll Cardiol 2018;71:1696-706.
6. Statello L, Guo CJ, Chen LL, et al. Gene regulation by long non-coding RNAs and its biological functions. Nat Rev Mol Cell Biol 2021;22:96-118.
7. Yao RW, Wang Y, Chen LL. Cellular functions of long noncoding RNAs. Nat Cell Biol 2019;21:542-51.
8. Lu D, Thum T. RNA-based diagnostic and therapeutic strategies for cardiovascular disease. Nat Rev Cardiol 2019;16:661-74.
9. Yang Z, Jiang S, Shang J, et al. LncRNA: Shedding light on mechanisms and opportunities in fibrosis and aging. Ageing Res Rev 2019;52:17-31.
10. Schulte C, Barwari T, Joshi A, et al. Noncoding RNAs versus Protein Biomarkers in Cardiovascular Disease. Trends Mol Med 2020;26:583-96.
11. Jaé N, Dimmeler S. Noncoding RNAs in Vascular Diseases. Circ Res 2020;126:1127-45.
12. Dong K, Shen J, He X, et al. CARMN Is an Evolutionarily Conserved Smooth Muscle Cell-Specific LncRNA That Maintains Contractile Phenotype by Binding Myocardin. Circulation 2021;144:1856-75.
13. Cai B, Ma W, Wang X, et al. Targeting LncDACH1 promotes cardiac repair and regeneration after myocardium infarction. Cell Death Differ 2020;27:2158-75.
14. Cai B, Zhang Y, Zhao Y, et al. Long Noncoding RNA-DACH1 (Dachshund Homolog 1) Regulates Cardiac Function by Inhibiting SERCA2a (Sarcoplasmic Reticulum Calcium ATPase 2a). Hypertension 2019;74:833-42.
15. Yang L, Deng J, Ma W, et al. Ablation of lncRNA Miat attenuates pathological hypertrophy and heart failure. Theranostics 2021;11:7995-8007.

16. Fasolo F, Jin H, Winski G, et al. Long Noncoding RNA MIAT Controls Advanced Atherosclerotic Lesion Formation and Plaque Destabilization. Circulation 2021;144:1567-83.
17. Li M, Zheng H, Han Y, et al. LncRNA Snhg1-driven self-reinforcing regulatory network promoted cardiac regeneration and repair after myocardial infarction. Theranostics 2021;11:9397-414.
18. Chen Y, Li S, Zhang Y, et al. The lncRNA Malat1 regulates microvascular function after myocardial infarction in mice via miR-26b-5p/Mfn1 axis-mediated mitochondrial dynamics. Redox Biol 2021;41:101910.
19. Liang H, Su X, Wu Q, et al. LncRNA 2810403D21Rik/Mirf promotes ischemic myocardial injury by regulating autophagy through targeting Mir26a. Autophagy 2020;16:1077-91.
20. Kay M, Soltani BM, Nemir M, et al. The conserved long noncoding RNA CARMA regulates cardiomyocyte differentiation. Cardiovasc Res 2021. [Epub ahead of print]. doi: 10.1093/cvr/cvab281.
21. Wu F, Huang W, Tan Q, et al. ZFP36L2 regulates myocardial ischemia/reperfusion injury and attenuates mitochondrial fusion and fission by LncRNA PVT1. Cell Death Dis 2021;12:614.
22. Tromp J, Ferreira JP, Janwanishstaporn S, et al. Heart failure around the world. Eur J Heart Fail 2019;21:1187-96.
23. Lindley KJ, Aggarwal NR, Briller JE, et al. Socioeconomic Determinants of Health and Cardiovascular Outcomes in Women: JACC Review Topic of the Week. J Am Coll Cardiol 2021;78:1919-29.
24. Taylor RS, Dalal HM, McDonagh STJ. The role of cardiac rehabilitation in improving cardiovascular outcomes. Nat Rev Cardiol 2022;19:180-94.
25. Terentes-Printzios D, Ioakeimidis N, Rokkas K, et al. Interactions between erectile dysfunction, cardiovascular disease and cardiovascular drugs. Nat Rev Cardiol 2022;19:59-74.
26. Han L, Yang L. Multidimensional Mechanistic Spectrum of Long Non-coding RNAs in Heart Development and Disease. Front Cardiovasc Med 2021;8:728746.
27. Xie L, Zhang Q, Mao J, et al. The Roles of lncRNA in Myocardial Infarction: Molecular Mechanisms, Diagnosis Biomarkers, and Therapeutic Perspectives. Front Cell Dev Biol 2021;9:680713.
28. Gao R, Wang L, Bei Y, et al. Long Noncoding RNA Cardiac Physiological Hypertrophy-Associated Regulator Induces Cardiac Physiological Hypertrophy and Promotes Functional Recovery After Myocardial Ischemia-Reperfusion Injury. Circulation 2021;144:303-17.
29. Luo S, Zhang M, Wu H, et al. SAIL: a new conserved anti-fibrotic lncRNA in the heart. Basic Res Cardiol 2021;116:15.
30. Hao K, Lei W, Wu H, et al. LncRNA-Safe contributes to cardiac fibrosis through Safe-Sfrp2-HuR complex in mouse myocardial infarction. Theranostics 2019;9:7282-97.
31. Fang Y, Sun B, Gao J, et al. LncRNA SLCO4A1-AS1 Accelerates Growth and Metastasis of Gastric Cancer via Regulation of the miR-149/XIAP Axis. Front Oncol 2021;11:683256.
32. Jin D, Huang K, Peng L, et al. Circular RNA circDNA2 upregulates CCDC6 expression to promote the progression of gastric cancer via miR-149-5p suppression. Mol Ther Nucleic Acids 2021;26:360-73.
33. Zhang X, Wang S, Wang H, et al. Circular RNA circNRIP1 acts as a microRNA-149-5p sponge to promote gastric cancer progression via the AKT1/mTOR pathway. Mol Cancer 2019;18:20.
34. Ouyang X, Feng L, Yao L, et al. Testicular orphan receptor 4 (TR4) promotes papillary thyroid cancer invasion via activating circ-FNLA/miR-149-5p/MMP9 signaling. Mol Ther Nucleic Acids 2021;24:755-67.
35. Qu L, Chen Y, Zhang F, et al. The lncRNA DLGAP1-AS1/miR-149-5p/TGFB2 axis contributes to colorectal cancer progression and 5-FU resistance by regulating smad2 pathway. Mol Ther Oncolytics 2021;20:607-24.
36. Meng X, Sun W, Yu J, et al. LINC00460-miR-149-5p/miR-150-5p-Mutant p53 Feedback Loop Promotes Oxaliplatin Resistance in Colorectal Cancer. Mol Ther Nucleic Acids 2020;22:1004-15.
37. Chen P, Yao Y, Yang N, et al. Circular RNA circCTNNA1 promotes colorectal cancer progression by sponging miR-149-5p and regulating FOXM1 expression. Cell Death Dis 2020;11:557.
38. Xiang F, Fan Y, Ni Z, et al. Ursolic Acid Reverses the Chemoresistance of Breast Cancer Cells to Paclitaxel by Targeting MiRNA-149-5p/MyD88. Front Oncol 2019;9:501.
39. Li Q, Li S, Xu C, et al. microRNA-149-5p mediates the PM2.5-induced inflammatory response by targeting TAB2 via MAPK and NF-κB signaling pathways in vivo and in vitro. Cell Biol Toxicol 2021. doi:10.1007/s10565-021-09638-5.
40. Zhang J, Ma Y, Zhang Y, et al. Angiogenesis is Inhibited by Arsenic Trioxide Through Downregulation of the CircHIPK3/miR-149-5p/FOXO1/VEGF Functional Module in Rheumatoid Arthritis. Front Pharmacol

2021;12:751667.
41. Yi E, Zhang J, Zheng M, et al. Long noncoding RNA IL6-AS1 is highly expressed in chronic obstructive pulmonary disease and is associated with interleukin 6 by targeting miR-149-5p and early B-cell factor 1. Clin Transl Med 2021;11:e479.
42. Ye ZM, Yang S, Xia YP, et al. LncRNA MIAT sponges miR-149-5p to inhibit efferocytosis in advanced atherosclerosis through CD47 upregulation. Cell Death Dis 2019;10:138.
43. Zhu S, Chen X, Wang JN, et al. Circular RNA circUbe2k promotes hepatic fibrosis via sponging miR-149-5p/TGF-β2 axis. FASEB J 2021;35:e21622.
44. Poller W, Dimmeler S, Heymans S, et al. Non-coding RNAs in cardiovascular diseases: diagnostic and therapeutic perspectives. Eur Heart J 2018;39:2704-16.
45. Bär C, Chatterjee S, Thum T. Long Noncoding RNAs in Cardiovascular Pathology, Diagnosis, and Therapy. Circulation 2016;134:1484-99.
46. Chen Y, Chen X, Li H, et al. Serum extracellular vesicles containing MIAT induces atrial fibrosis, inflammation and oxidative stress to promote atrial remodeling and atrial fibrillation via blockade of miR-485-5p-mediated CXCL10 inhibition. Clin Transl Med 2021;11:e482.
47. Feng Y, Xu W, Zhang W, et al. LncRNA DCRF regulates cardiomyocyte autophagy by targeting miR-551b-5p in diabetic cardiomyopathy. Theranostics 2019;9:4558-66.
48. Koch M, Schulze J, Hansen U, et al. A novel marker of tissue junctions, collagen XXII. J Biol Chem 2004;279:22514-21.
49. Charvet B, Guiraud A, Malbouyres M, et al. Knockdown of col22a1 gene in zebrafish induces a muscular dystrophy by disruption of the myotendinous junction. Development 2013;140:4602-13.
50. Watanabe T, Baker Frost DA, Mlakar L, et al. A Human Skin Model Recapitulates Systemic Sclerosis Dermal Fibrosis and Identifies COL22A1 as a TGFβ Early Response Gene that Mediates Fibroblast to Myofibroblast Transition. Genes (Basel) 2019;10:75.

(English Language Editor: L. Huleatt)

Cite this article as: Li X, Teng Y, Tian M, Qiu H, Zhao J, Gao Q, Zhang Y, Zhuang J, Chen J. Enhancement of LncRNA-HFRL expression induces cardiomyocyte inflammation, proliferation, and fibrosis via the sequestering of miR-149-5p-mediated collagen 22A inhibition. Ann Transl Med 2022;10(9):523. doi: 10.21037/atm-22-1756

